Observation of magnetic rotation in odd-odd ^{104}Ag

P. Datta
Department of Physics, Ananda Mohan College, Kolkata 700 009, India

S. Chattopadhyay, P. Banerjee, S. Bhattacharya, B. Dasmahapatra, T. K. Ghosh, A. Goswami, S. Pal, M. Saha Sarkar, and S. Sen
Saha Institute of Nuclear Physics, 1/AF Bidhan Nagar, Kolkata 700 064, India

H. C. Jain and P. K. Joshi
Tata Institute of Fundamental Research, Homi Bhabha Road, Mumbai 400 005, India

Amita
Department of Physics, RBS College, Agra 282 002, India
(Received 9 January 2004; published 27 April 2004)

The high spin level structure of ^{104}Ag has been extended to $I^{\pi}=20^{+}$ and excitation energy of 7.159 MeV through the discrete line γ-ray spectroscopy. The negative parity ground state band has been confirmed and extended to $I^{\pi}=18^{-}$. Two new nonyrast dipole bands, one with positive and the other with negative parity, have been observed. The parities of the two bands have been established through polarization directional correlation measurement of the feed-out transitions from these bands. The level lifetimes have been measured in the ground state band and the positive parity dipole band. The measured total angular momenta and the $B(M1)$ rates have been compared with the predictions of hybrid version of the tilted axis cranking. The $B(M1)$ rates have also been compared with the values obtained from Dönau's geometric formula. The tilted axis calculations give good overall agreement which suggests that all the three bands of ^{104}Ag exhibits magnetic rotation.

DOI: 10.1103/PhysRevC.69.044317 PACS number(s): 27.60.+j, 21.10.Re, 21.10.Hw, 21.60.Ev

I. INTRODUCTION

The magnetic rotation has been observed in nuclei having small deformations and is characterized by a $\Delta I=1$ rotational structure rather than a $\Delta I=2$ structure. Thus, the intraband transitions are predominantly magnetic dipole ($M1$) in nature while the crossover $E2$ transitions are either weak or absent. In addition, these bands exhibit smaller dynamical moments of inertia compared to those of normally deformed nuclei and have high K values (projection of total angular momentum on symmetry axis) for the bandheads which implies multiquasiparticle configurations.

In the case of magnetic rotation, the angular momentum is generated by gradual alignment of spins of the deformation-aligned and the rotation-aligned quasiparticles and the angular momentum is not along any of the principal axes of the nucleus. The theoretical explanation for the bands which originates due to magnetic rotation ($M1$ bands) has been provided by the tilted axis cranking (TAC) [1] model. In mass-100 region, the $M1$ bands have been observed for configurations where the quasiprotons are in high Ω orbitals of $[g_{9/2}]$ while the quasineutrons occupy the low Ω orbitals of $[h_{11/2}]$. A large number of $M1$ bands have been observed in the even-even and odd mass nuclei mass-100 region ($45 \leqslant Z \leqslant 50$ and $N>50$) [2–8]. However, only recently, $M1$ bands have been reported in odd-odd ^{108,110}In isotopes [9].

In the previous study of ^{104}Ag, a strongly coupled yrast band with $\pi g_{9/2} \otimes \nu h_{11/2}$ configuration has been reported [10,11]. The present work suggests significant extension in the level scheme of ^{104}Ag and two new nonyrast dipole bands have been identified. A comparison between the observed characteristics of the three bands and the results of TAC calculations seems to suggest that all the three bands of ^{104}Ag originate due to magnetic rotation.

II. EXPERIMENT

The high spin states of ^{104}Ag were populated through ^{76}Ge(^{35}Cl, $\alpha 3n\gamma$)^{104}Ag reaction using the 132 MeV ^{35}Cl beam from the 14-UD Pelletron at TIFR. The target was prepared by evaporating $\sim$700 μg/cm^2 of 99.8% enriched ^{76}Ge on 10 mg/cm^2 Au foil. The γ rays were detected by an array consisting of eight Compton suppressed Clover detectors [12], which were placed in the horizontal plane at 60°, 90°, 120°, 150°, 215°, 255°, 285°, and 325° with respect to the beam direction. The present geometry allows the polarization measurements of the observed γ rays using the Clover detectors.

A total of 200×10^6 threefold coincidences were collected.

III. ANALYSIS METHOD

The data were sorted in the following four different matrices by unfolding each threefold coincidence event into three twofold events with a time gate of 100 ns. The symmetric matrix was analyzed with the RADWARE program ESCL8R [13] while all the asymmetric matrices were analyzed using RADWARE program SLICE [13].

(1) The symmetrized E_γ-E_γ matrix: This was used to generate various gated spectra.

(2) The asymmetric angular correlation matrix: This was formed in order to determine the directional correlation orientation (DCO) ratios, defined as

$$R_{\mathrm{DCO}} = \frac{I_\gamma(\text{observed at } 150\,^\circ,\ 215\,^\circ, \text{ and } 325\,^\circ, \text{ gate on } 90\,^\circ,\ 255\,^\circ, \text{ and } 285^\circ)}{I_\gamma(\text{observed at } 90\,^\circ,\ 255\,^\circ, \text{ and } 285\,^\circ, \text{ gate on } 150\,^\circ,\ 215\,^\circ, \text{ and } 325^\circ)}, \tag{1}$$

which were compared with the theoretical DCO ratios for spin assignments.

(3) The asymmetric PDCO matrices: Two asymmetric matrices were sorted in order to determine the electromagnetic nature (electric or magnetic) of the γ rays by the polarization directional correlation (PDCO) method [14]. In this method, the asymmetry of Compton-scattered polarized photon was calculated from the expression

$$A = \frac{aN(90\,^\circ) - N(0\,^\circ)}{aN(90\,^\circ) + N(0\,^\circ)}, \tag{2}$$

where $N(90°)$ and $N(0°)$ denote the number of γ rays with scattering axis perpendicular and parallel to the emission plane and a is the correction term due to the asymmetry in response to the Clover segments. It is defined as

$$a = \frac{N(0°)(\text{unpolarized})}{N(90°)(\text{unpolarized})}, \tag{3}$$

and is measured as a function of energy with a radioactive source. For the present array, the energy dependence of the correction term was determined with ^{152}Eu and ^{66}Ga ($T_{1/2}$ = 9.41 h) sources. The ^{66}Ga source was prepared through ^{52}Cr(^{16}O,pn)^{66}Ga reaction [12]. With this source the value of a could be measured up to 2752 keV. Figure 1 shows that the correction term, over this long energy range, is nearly constant and has a value close to 1.0.

One of the PDCO matrices was constructed by placing the events along one axis (x axis) recorded in the two segments which are parallel to the emission plane while the coincident γ ray was placed on the other axis (y axis). The other matrix was formed in a similar way but in this case, events from the segments of the Clover detectors which were perpendicular with respect to the emission plane were considered. According to the present definition, a negative PDCO value would imply a magnetic transition while a positive value corresponds to an electric transition.

(4) The asymmetric Doppler-Shift attenuation method (DSAM) matrices: Three asymmetric DSAM matrices were constructed to perform the line shape analysis. These matrices were constructed by placing events recorded at a specific angle (60°, 120°, and 90°) on x axis while events recorded at all other angles were placed on y axis. The line shapes were observed above $I = 13\hbar$ at both forward and backward angles by putting gates on the y axis and projecting the spectra on the x axis. The lifetimes of different states of ^{104}Ag were measured by fitting these experimental line shapes with the LINESHAPE analysis code developed by Wells and Johnson [15].

IV. RESULTS

A. Level scheme

The partial level scheme of ^{104}Ag (shown in Fig. 2) has been established using the relative intensities of γ rays in various γ gates, the DCO and PDCO ratios. The present work confirms the level scheme established in the earlier works [10,11]. The portions of the level scheme which has been extended or modified are discussed below. The relative intensities of γ rays below $I^\pi = 11^-$ state were estimated from gates on the symmetrized E_γ-E_γ matrix, while the relative intensities of the γ rays which exhibit line shapes at forward and backward angles were obtained from the gated spectra at 90°. The intensities for the $\Delta I = 1$ and $\Delta I = 2$ transitions in the gated spectra at 90° were obtained by normalizing them with respect to the intensities of the 346 and 678 keV transitions, respectively, which have been estimated from the symmetrized E_γ-E_γ matrix.

Band 1. It is a negative parity band with bandhead at $I^\pi = 8^-$ which predominantly decays to the $I^\pi = 7^+$ state through the 865 keV transition. All the transitions reported earlier [10,11] have been reconfirmed except for the 570 keV γ ray which deexcites 17^- level. This transition energy has been modified to 572 keV and this change is supported by the presence of the corresponding crossover $E2$ transition of 1092 keV. This band has been extended to $I = 18\hbar$ through

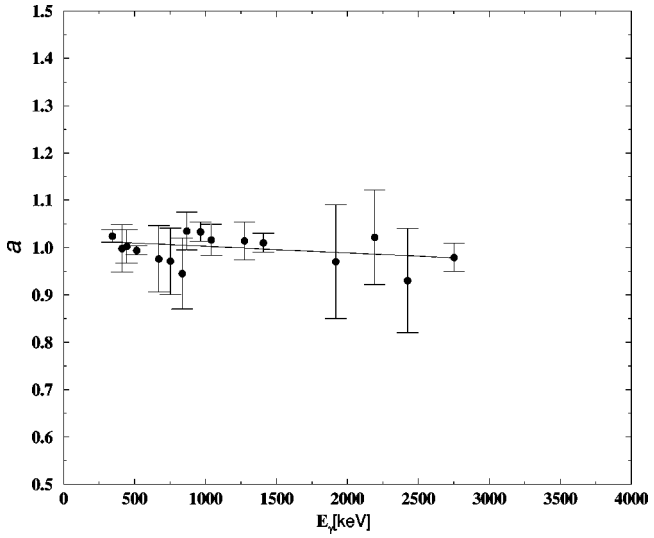

FIG. 1. Correction factor a defined in Eq. (3) as a function of γ-ray energy for the Clover detector array. The solid line shows the best χ^2 fit to the data points which give the parametric dependence of the correction term on the γ energy.

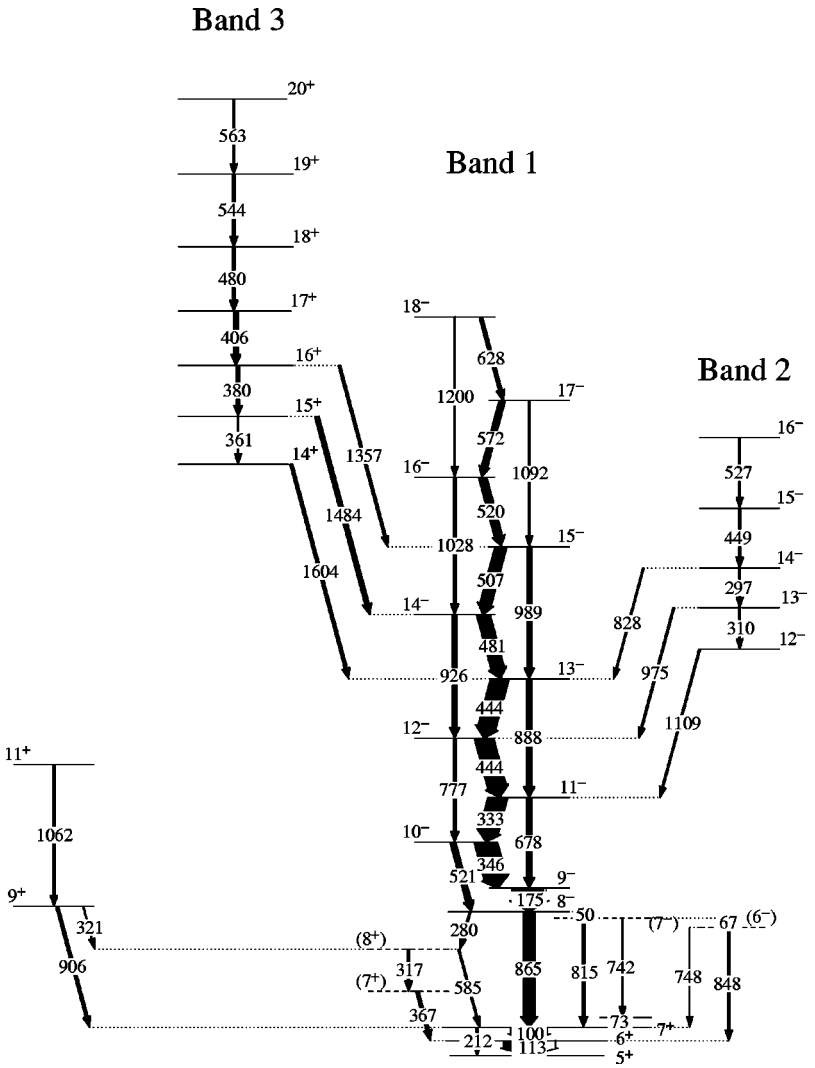

FIG. 2. Partial level scheme of ^{104}Ag. The γ transition energies are in keV.

the placement of an $M1$ transition of energy 628 keV. The crossover $E2$ transition of 1200 keV has also been identified.

The intensity of the 444 keV transition which deecxcites 13^- level has been determined from the 777 keV gated spectrum while the intensity of the lower 444 keV transition has been estimated by subtracting the intensity of upper 444 keV transition from the observed intensity of the 444 keV transition in 175 keV gate.

The DCO values have been extracted from the DCO matrices using the 175 keV and 346 keV gates and have been tabulated in Table I. In the present setup, the measured DCO ratio for 175 keV transition in the $E2$ gate of 678 keV was found to be 0.62. This value was reproduced by theoretical calculations where the value of the spin alignment parameter σ_I/I and the mixing ratio δ were assumed to be 0.35 and 0.02, respectively. The value of δ is consistent with the previous measurement [10]. The calculated DCO ratios for various combinations of multipolarities for the present array are listed in Table II. The multipolarities of the transitions and the spins of the energy levels in ^{104}Ag have been obtained by comparing the measured DCO ratios with the theoretical values listed in Table II.

The electric and the magnetic characters of the observed transitions were determined through the PDCO measurements. The PDCO values have been extracted from the PDCO matrices using the above-mentioned gates and are tabulated in Table I. The measured PDCO values for different γ rays have been plotted in Fig. 3 which shows that the previously reported $E2$ and $M1$ transitions have positive and negative PDCO values, respectively. The error bars on the measured values correspond to 90% confidence since these errors were estimated by considering the extreme possible values of $N(0°)$ and $N(90°)$.

The 175 and 444 keV gates belonging to Band 1 are shown in Fig. 4. In the 175 keV gate, there are some high energy transitions which do not show any appreciable line shapes. These transitions of 1357, 1484, and 1604 keV are shown in the inset of Fig. 4(a). The DCO and PDCO values of these transitions (given in Table I) establish them as $E1$ transitions. This assignment is consistent with absence of line shapes, indicating long lifetimes expected for $E1$ transitions. These transitions, therefore, provide the crucial connections to the nonyrast positive parity band of ^{104}Ag.

In addition, three more γ transitions with energies 828, 975, and 1109 keV were observed in the 175 keV gate. The DCO and PDCO values establish the $M1$ character for these transitions. These transitions are the feed-out transitions from the nonyrast negative parity band of ^{104}Ag.

TABLE I. Relative intensities, DCO and PDCO ratios for γ transitions of energy E_γ which deexcite the energy levels E_i in ^{104}Ag. Unless otherwise mentioned, the values in column 5 are obtained from gate on pure dipole (D) 175 keV transition.

E_γ (keV)	E_i (keV)	$I_i^\pi \rightarrow I_f^\pi$	Relative intensity	$R_{DCO}(D)$	PDCO
100	212	$7^+ \rightarrow 6^+$	65.0(6.0)		
113	339	$6^+ \rightarrow 5^+$	100.0(9.0)		
175	1253	$9^- \rightarrow 8^-$	78.0(3.1)		
212	212	$7^+ \rightarrow 5^+$	5.3(1.0)		
280	1078	$(8^-) \rightarrow (8^+)$	4.1(1.0)		
297	3648	$15^- \rightarrow 14^-$	3.9(0.4)	0.89(0.12)[a]	−0.069(0.084)
310	3351	$14^- \rightarrow 13^-$	3.6(0.4)	0.89(0.12)	
317	797	$(8^+) \rightarrow (7^+)$	5.7(1.0)		
321	1118	$(9^+) \rightarrow (8^+)$	1.9(0.4)		
333	1931	$11^- \rightarrow 10^-$	47.6(2.0)	0.94(0.04)	−0.077(0.042)
346	1599	$10^- \rightarrow 9^-$	55.9(2.4)	0.93(0.04)	−0.003(0.038)
361	4785	$15^+ \rightarrow 14^+$	4.2(0.5)	1.06(0.12)	
367	480	$(7^+) \rightarrow (6^+)$	7.9(1.0)		
380	5165	$16^+ \rightarrow 15^+$	8.3(0.6)	0.99(0.10)	
406	5571	$17^+ \rightarrow 16^+$	12.0(0.9)	0.96(0.08)	−0.088(0.072)
444	2376	$12^- \rightarrow 11^-$	46.7(3.1)	0.93(0.03)	−0.021(0.031)
444	2820	$13^- \rightarrow 12^-$	44.9(2.9)	0.93(0.03)	−0.021(0.031)
449	4097	$16^- \rightarrow 15^-$	5.4(0.5)	0.97(0.14)[a]	
480	6051	$18^+ \rightarrow 17^+$	7.8(0.8)		
481	3301	$14^- \rightarrow 13^-$	33.1(3.1)		
507	3808	$15^- \rightarrow 14^-$	28.8(1.4)	0.97(0.06)	−0.040(0.037)
520	4328	$16^- \rightarrow 15^-$	20.1(1.3)	0.94(0.07)[a]	−0.079(0.061)
521	1599	$10^- \rightarrow 8^-$	14.1(1.1)		
527	4624	$17^- \rightarrow 16^-$	4.0(0.4)		
544	6595	$19^+ \rightarrow 18^+$	6.5(0.5)		
563	7159	$20^+ \rightarrow 19^+$	5.8(0.4)		
572	4901	$17^- \rightarrow 16^-$	15.3(1.0)	0.85(0.08)[a]	−0.029(0.030)
585	797	$8^+ \rightarrow 7^+$	4.1(0.8)		
628	5528	$18^+ \rightarrow 17^+$	8.3(0.7)		
678	1931	$11^- \rightarrow 9^-$	14.1(1.0)	1.41(0.13)	0.018(0.070)
742	1078		3.6(0.4)		
748	960	$(6^-) \rightarrow 7^+$	1.7(0.5)		
777	2376	$12^- \rightarrow 10^-$	8.2(0.7)		0.108(0.068)
815	1078	$(7^-) \rightarrow 7^+$	7.6(1.0)	1.01(0.9)	
828	3647	$15^- \rightarrow 13^-$	3.4(0.5)	0.98(0.15)	−0.063(0.097)
848	960	$(6^-) \rightarrow 6^+$	6.0(0.8)		
865	1078	$8^- \rightarrow 7^+$	30.0(2.0)	0.97(0.07)[a]	0.077(0.048)
888	2820	$13^- \rightarrow 11^-$	15.5(1.2)	1.36(0.13)[a]	
906	1118	$(9^+) \rightarrow 7^+$	7.0(1.0)	1.58(0.21)[a]	
926	3301	$14^- \rightarrow 12^-$	11.7(1.0)	1.47(0.17)[a]	0.053(0.082)
975	3351	$(14^-) \rightarrow 12^-$	4.2(0.6)		
989	3808	$15^- \rightarrow 13^-$	12.0(1.1)	1.42(0.16)[a]	
1028	4328	$16^- \rightarrow 14^-$	7.1(1.0)	1.55(0.17)[a]	0.138(0.088)
1092	4901	$17^- \rightarrow 15^-$	4.7(0.6)	1.60(0.23)	
1109	3041	$13^- \rightarrow 11^-$	4.0(0.5)	0.95(0.12)	−0.055(0.118)
1200	5528	$18^- \rightarrow 16^-$	3.6(0.4)	0.91(0.12)	

TABLE I. (*Continued.*)

E_γ (keV)	E_i (keV)	$I_i^\pi \rightarrow I_f^\pi$	Relative intensity	$R_{DCO}(D)$	PDCO
1357	5165	$16^+ \rightarrow 15^-$	6.0(0.9)	0.97(0.20)[a]	0.096(0.109)
1484	4785	$15^+ \rightarrow 14^-$	10.9(1.2)	0.88(0.11)[a]	0.109(0.086)
1604	4424	$14^+ \rightarrow 13^-$	7.2(1.0)	0.87(0.14)	0.132(0.116)

[a]R_{DCO} from gate on 346 keV transition.

Band 2. This is a negative parity nonyrast band with bandhead at $I^\pi = 12^-$. This band feeds Band 1 through three $M1$ transitions of energies 828, 975, and 1109 keV. The level energies of this band could be fixed accurately due to the presence of these three transitions along with the intraband transitions of 297 and 310 keV. Figure 5(a) shows the 297 keV gate where the two feed-out transitions of 975 and 1109 keV are visible. In addition to the transitions belonging to the Band 1, two more transitions of energies 449 and 527 keV were found to be in coincidence with 297 and 310 keV transitions. These transitions have been placed above the 14^- level according to their intensities. Thus, Band 2 consists of four $M1$ transitions of 310, 297, 449, and 527 keV and no crossover $E2$ transition could be observed.

Band 3. This is a positive parity band with bandhead at $I^\pi = 14^+$. This band feeds Band 1 through three $E1$ transitions of energies 1357, 1484, and 1604 keV. In this band also, there is a large degree of correlation in the lower part of the band, which helps in fixing the level energies accurately. The three feed-out transitions are shown in the inset of Fig. 5(b) which shows the 406 keV gate. This band consists of six $M1$ transitions which have been placed according to their observed intensities. In this band also no crossover $E2$ transitions could be observed.

B. DSAM analysis

The line shapes were extracted by putting gates on the y axis of each of the three DSAM matrices and the Doppler broadened line shapes were identified at forward 60° and backward 120° angles with respect to the beam direction, by comparing these spectra with those obtained at 90°.

In ^{104}Ag, line shapes were observed in Band 1 and Band 3 above $I^\pi = 13^-$ and $I^\pi = 16^+$, respectively. For each of the above-mentioned angles, the level lifetimes of the two bands were measured using LINESHAPE analysis codes of Wells and Johnson [15]. These codes were used to generate the velocity profile of the recoiling nuclei into the backing using Monte Carlo technique with a time step of 0.001 ps for 5000 histories. These profiles were generated at 60° and 120°. Electronic stopping powers of the Northcliffe and Shilling [16] corrected for shell effects were used for calculating the energy loss.

The energies of γ transitions and the side-feeding intensities were extracted from the 90° spectra. These values were used as input parameters for the line shape analysis. The side feeding into each level and feeding to the topmost level of each band were initially modeled as a cascade of five transitions with a moment of inertia which is comparable to that of the band of interest. The quadrupole moments of the side-feeding sequences were allowed to vary which when combined with the moment of inertia gave an effective side-feeding lifetime parameters for each level. For every observed line shape, in-band and side-feeding lifetimes, background parameters and the intensities of the contaminant peaks were allowed to vary. The energies of the contaminant peaks were fixed from the 90° spectra. For each set of the parameters the simulated line shapes were fitted to experimental spectra using χ^2-minimization routines of MINUIT [17].

For each band, the lifetime measurements were performed starting with the topmost transition which was assumed to have 100% side feed. The other parameters were allowed to vary until the minimum χ^2 was reached. The background and the stopped contaminant peak parameters for the best fit were then fixed. Thus, the line shape analysis for the topmost transition led to the estimation of the effective lifetime for the topmost level. For the next lower level, the effective lifetime

TABLE II. Calculated DCO ratios for the present array for different types of transitions considering spin alignment parameter $\sigma_I/I = 0.35$.

Multipolarity	$I_i \rightarrow I_f$	Gating transition $\Delta I = 2$ (stretched) R_{DCO}	Gating transition $\Delta I = 1$ ($\delta = 0.02$) R_{DCO}
Quadrupole (stretched)	$I \rightarrow I-2$	1.0	1.57
Dipole (stretched)	$I \rightarrow I-1$	0.60	0.97
Dipole ($\delta > 0$)	$I \rightarrow I-1$	>0.60	>0.97
Dipole ($\delta < 0$)	$I \rightarrow I-1$	<0.60	<0.97

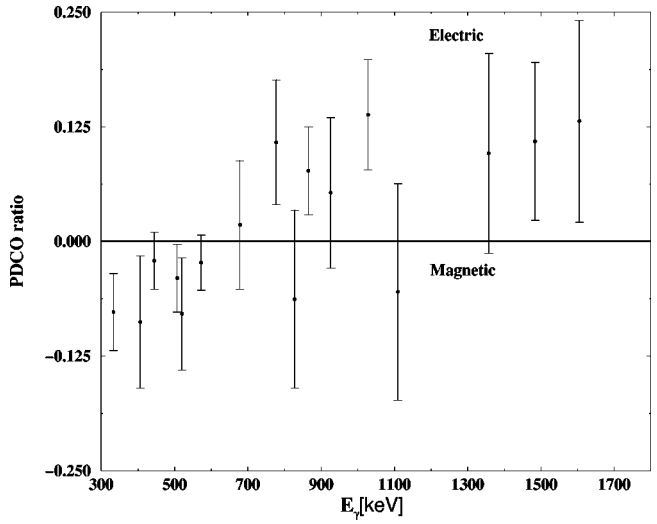

FIG. 3. The measured PDCO values [as defined in Eq. (2)] for different γ transitions in ^{104}Ag.

of the topmost level and the side-feeding lifetime were considered effective time parameters. In this way, each lower level was then added one by one and fitted, until the entire band was included in a global fit where only the in-band and side-feeding lifetimes were allowed to vary. This procedure of global fit was then repeated for the forward and backward angles. The error bar on the lifetime values includes the fitting error and the error in the side-feeding intensity. However, the systematic error in the stopping power values which has not been included may be as large as 10%.

The lifetime values obtained for each level at these two angles were found to agree within the limits of error and the final values for the lifetimes were obtained by taking averages from the fits at these two angles. The examples of line shape fits for four γ transitions are shown in Fig. 6. The fitted line shapes are drawn with solid lines while the contaminant peaks are shown in dots. The 90° spectra have been shown as references so as to identify the line shapes at the forward and backward angles.

For each band, $B(M1)$ and $B(E2)$ transition rates have been calculated using the equations given in Ref. [9]. The measured lifetimes along with the corresponding $B(M1)$ and $B(E2)$ values have been listed in Table III. In estimating the $B(M1)$ values, the mixing ratio $\delta=0$ was assumed for all the $\Delta I=1$ transition.

The line shapes for Band 1 were extracted from the 346 keV gate while for Band 3 the 1484 keV gate were used. These two gates had the minimum number of contaminant lines in the projected spectra. The present data are insufficient to extract any line shape in Band 2.

It was estimated using LINESHAPE code that for the present target-projectile combination, if the effective lifetime of a level exceeds 4 ps then the corresponding γ transition does not show any significant line shape. Thus, it can be concluded that the effective lifetimes for the 14^+, 15^+, and 16^+ levels of Band 3 are more than 4 ps.

In the 346 keV gated spectrum, the 481 keV transition of Band 1 and 480 keV transition of Band 3 both exhibit line shapes which overlap with each other. However, it is interesting to note that 481 keV transition will not exhibit any line shape in 1484 keV gate. This is due to the fact that in this gate, the 14^- level is only fed by the 15^+ level which has an effective lifetime of more than 4 ps. Thus, the 481 keV

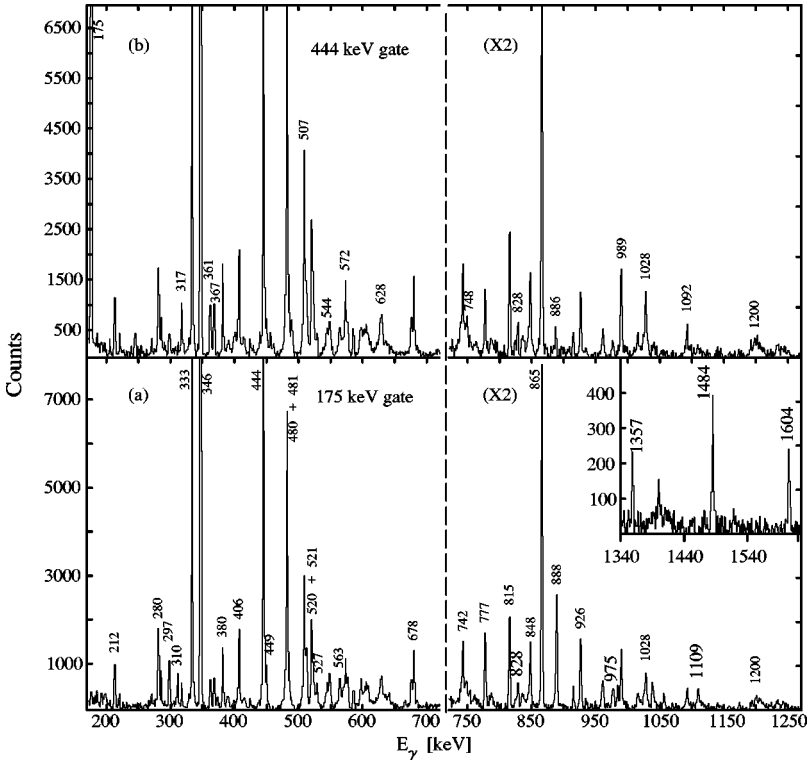

FIG. 4. γ-γ coincidence spectra with (a) 175 and (b) 444 keV gates in ^{76}Ge(^{35}Cl, $\alpha 3n\gamma$)^{104}Ag reaction. The counts beyond 720 keV have been scaled up by a factor of 2. The inset shows three high energy γ transitions observed in the 175 keV gate.

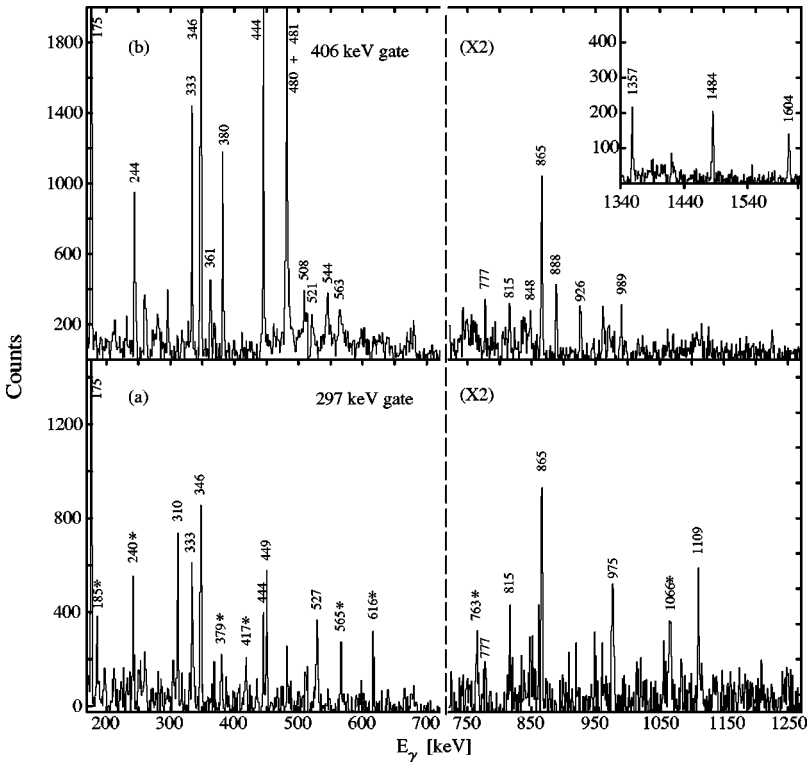

FIG. 5. γ-γ coincidence spectra with the (a) 297 and (b) 406 keV gates belonging to Band 2 and Band 3, respectively. The contaminant γ transitions from ^{105}Ag in 297 keV gate have been marked by asterisk.

transition is assumed to be a contaminant stopped peak in the line shape analysis of 480 keV transition. The intensity of the 481 keV peak was fixed in accordance to the observed intensity ratio of 480 and 481 keV transitions in the 1484 keV gated spectrum at 90°. This line shape and the fitted shape are shown in Fig 6.

The 481 keV line shape was extracted from the 520 keV gate so as to avoid the contamination in line shape from the 480 keV transition. In fitting this line shape, the lifetimes for the 17^-, 16^-, and 15^- levels have been kept fixed to the values extracted from the 346 keV gate and no side-feeding intensities have been considered for 15^- and 14^- levels.

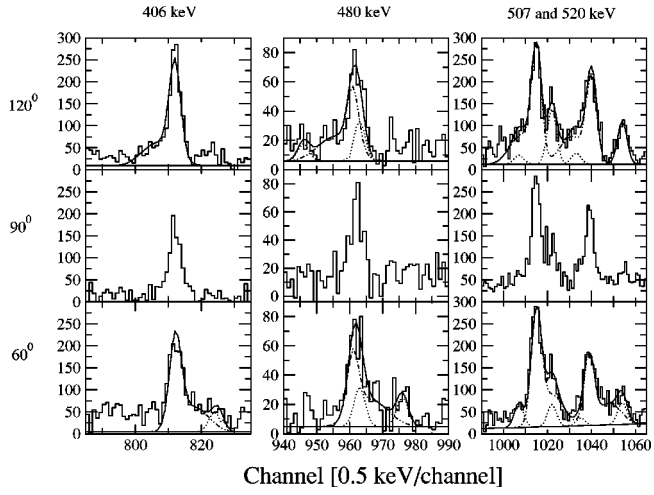

FIG. 6. Experimental and theoretical line shapes for the 406, 480, 507, and 520 keV γ rays at the forward 60° and backward 120° angles with respect to the beam direction. The contaminant peaks are shown by dotted lines and theoretical line shapes are shown by solid lines. The 90° spectra are shown in order to identify the line shapes and the contaminant peaks.

V. DISCUSSIONS

The negative parity ground state band (Band 1) of odd-odd ^{104}Ag is expected to be built on the $\pi g_{9/2} \otimes \nu h_{11/2}$ configuration where the odd neutrons occupy the negative parity high j intruder orbital. The ground state bands of the neighboring odd-odd ^{108,110}In [9] also have the same configuration. In Fig. 7, the aligned angular momentum i_x of Band 1 has been plotted as a function of rotational frequency ω. The reference parameters for i_x were assumed to be $\Im_0 = 7.0\hbar^2/\mathrm{MeV}$ and $\Im_1 = 15.0\hbar^4/\mathrm{MeV}^3$ [18]. The figure shows that there is a slow alignment around $\hbar\omega = 0.5$ MeV and the alignment gain is $\sim 3\hbar$. It is highly improbable to align protons across the $N=50$ shell gap. In addition, the AB crossing for the proton sector is blocked.

TABLE III. Measured level lifetimes and the corresponding $B(E1)$ and $B(E2)$ rates in ^{104}Ag. The error bars on measured lifetimes include the fitting errors and errors in side-feeding intensities.

Band	$E_I(I^\pi)$ (keV)	τ (ps)	$B(M1)$ μ_n^2	$B(E2)$ $(eb)^2$
	$3301(14^-)$	0.30 (6)	1.25 (30)	0.104 (25)
1	$3808(15^-)$	0.32 (6)	0.97 (21)	0.079 (17)
	$4328(16^-)$	0.35 (6)	0.86 (20)	0.053 (13)
	$5571(17^+)$	0.39 (7)	2.18 (43)	
3	$6051(18^+)$	0.30 (6)	1.71 (38)	
	$6595(19^+)$	0.28 (4)	1.26 (21)	

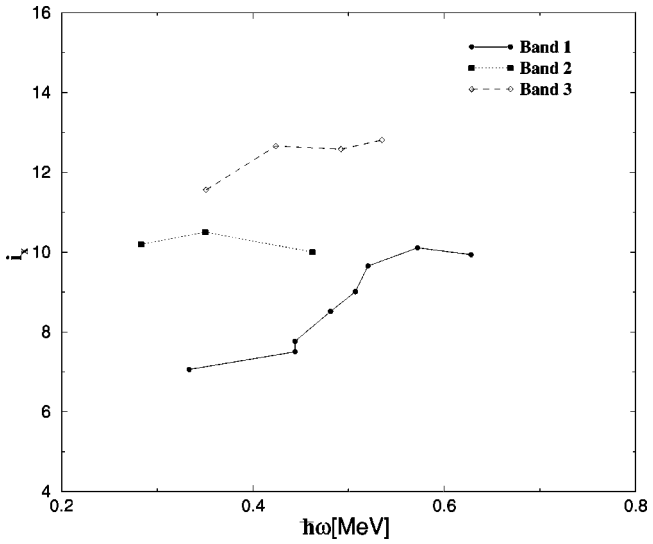

FIG. 7. Aligned angular momentum as a function of rotational frequency for Bands 1, 2, and 3. The experimental frequency is extracted from the measured γ energies using the relation $\hbar\omega(I) = E_\gamma = E(I) - E(I-1)$. The reference parameters were assumed to be $\Im_0 = 7.0\hbar^2/\mathrm{MeV}$ and $\Im_1 = 15.0\hbar^4/\mathrm{MeV}^3$[18].

The quasineutron Routhian for ^{104}Ag have been calculated using cranked shell model (CSM) with BCS pairing [19]. The calculated Routhian for $\beta_2 = 0.17$ and $\gamma = 29°$ is shown in Fig. 8 where $\gamma = 0°$ and 90° correspond to axial prolate and oblate shapes, respectively. These deformation parameters for $\pi g_{9/2} \otimes \nu h_{11/2}$ configuration were obtained by minimizing the total Routhian at $\hbar\omega = 0.3$ MeV. It is to be noted that for $\pi g_{9/2} \otimes \nu h_{11/2}$ configuration, the odd quasineutron blocks the *EF* crossing. The CSM calculations predict that the *AB* crossing occurs at $\hbar\omega \approx 0.55$ MeV and the gain in alignment $\sim 3\hbar$. These values are in good agreement with the observed values as shown in Fig. 7. Thus, the quasineutrons have *ABE* configuration for Band 1 after the observed alignment.

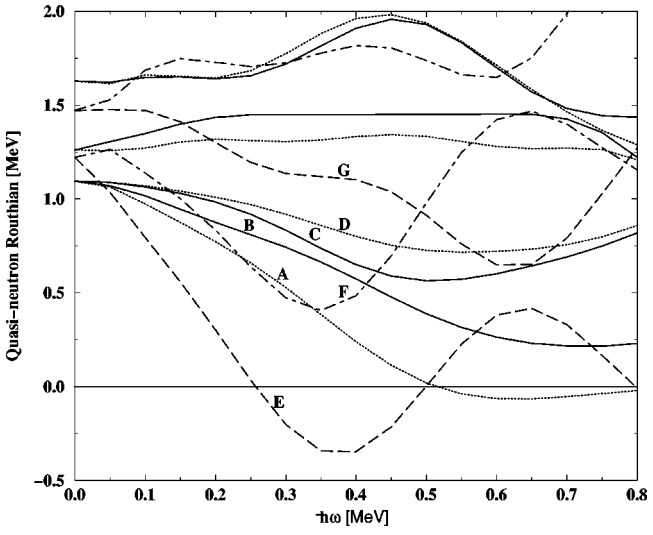

FIG. 8. Quasiparticle Routhian for neutrons in ^{104}Ag. Calculations are performed for $\beta_2 = 0.17$, $\beta_4 = 0.0$, and $\gamma = 29°$, where $\gamma = 0°$ corresponds to axial prolate shape and $\gamma = 90^\circ$ corresponds to axial oblate shape.

It is interesting to note that the aligned angular momentum for Band 2 is $\sim 10\hbar$ which is the same as that of Band 1 after alignment (Fig. 7). Thus, Band 2 is a four quasiparticle band since for two or six quasiparticle configurations, the value of the aligned angular momentum would not have matched so closely. In addition, the Bands 1 and 2 have the same parity. Thus, there are two possible negative parity four quasiparticle configurations for this band, namely, $\pi[g_{9/2}] \otimes \nu[(h_{11/2})^3]$ and $\pi[g_{9/2}] \otimes \nu[(g_{7/2}\, d_{5/2})^2 (h_{11/2})]$ with the neutron in unfavored $h_{11/2}$ orbital (that is, *ABF* configuration for quasineutrons). The CSM calculations predict that the aligned angular momentum for $\nu(h_{11/2})^3$ configuration (*EFG*) is $\sim 10\hbar$ higher than that of $\nu[(g_{7/2}d_{5/2})^2(h_{11/2})]$ configuration (*ABE*). So the first possibility seems improbable. However, the aligned angular momenta for *ABF* and *ABE* configurations are very similar. Thus, the probable quasineutron configuration for Band 2 is *ABF*.

The aligned angular momentum for Band 3 is $\sim 3\hbar$ higher than that of *ABE* configuration and has positive parity. Thus, probable quasineutron configuration for this band is *AEF* as it is consistent with the above-mentioned observations.

The observed features in the level scheme of ^{104}Ag have also been investigated using the hybrid version of TAC [20,21]. In this model, the spherical part of the single particle energies is taken from the spherical Woods-Saxon potential and combined with the deformed part of the anisotropic harmonic oscillator. This approximation has the advantage of using a realistic flat bottom potential. The gap parameter Δ was chosen as the 0.8 times the experimental odd-even mass difference Δ_{oe}, for protons and neutrons. The Δ_{oe} was calculated using the expression given in Ref. [22] with binding energies taken from the atomic mass table [23]. The chemical potentials for protons and neutrons were chosen to reproduce the correct proton and neutron numbers for ^{104}Ag.

A. Band 1

The high spin behavior of this decoupled band has been investigated within the framework of particle-rotor model (PRM) with variable moment of inertia [24] by Goswami *et al.* [11]. The calculations were based on $\pi g_{9/2} \otimes \nu h_{11/2}$ configuration and the quadrupole deformation was assumed to be $\beta_2 = 0.15$. The results of the calculations showed that the relative excitation energies of the level of Band 1 are in reasonable agreement with the corresponding experimental values. The observed branching ratios could also be reproduced by PRM calculation.

In the present work, the experimental data for Band 1 have also been compared with TAC calculation using the same parameters which were used for the CSM calculations.

In Fig. 9(a), the observed spins I of Band 1 have been plotted as a function of rotational frequency ω, where $\hbar\omega(I) = E(I) - E(I-1)$. The calculated $I(\omega)$ curve is shown in the figure by dotted lines. The good agreement between experiment and theory is apparent in the figure. The observed *AB* alignment and the alignment gain are well reproduced by TAC calculations.

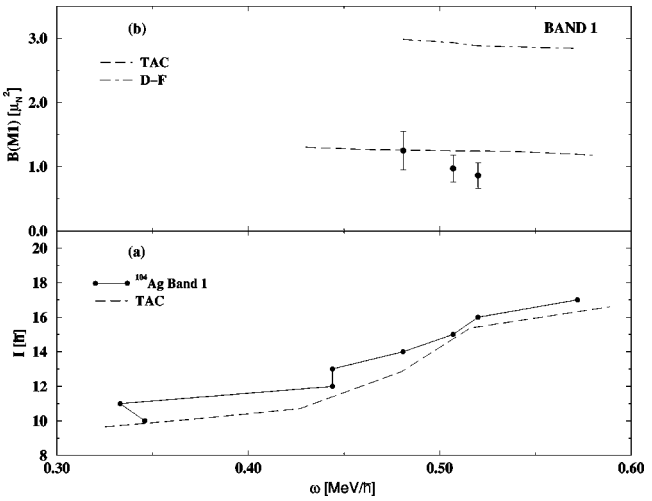

FIG. 9. (a) Angular momentum and (b) $B(M1)$ transition rates as a function of rotational frequency for Band 1. The dashed line in (a) denotes the theoretical values from TAC calculation for the assigned configuration of Band 1. The dashed and the dot-dashed lines in (b) represent the calculated $B(M1)$ rates from TAC and D-F formalism, respectively.

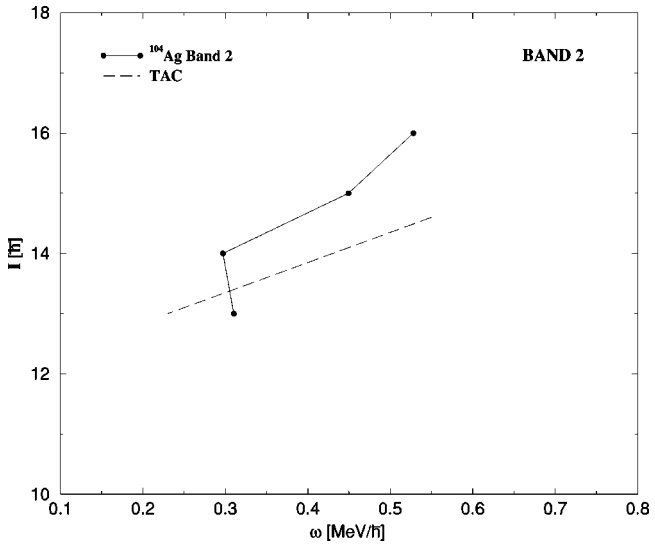

FIG. 10. Angular momentum as a function of rotational frequency for Band 2. The calculated values are shown by the dotted line.

In Fig. 9(b), the $B(M1)$ strengths calculated from the fitted lifetimes are plotted as a function of frequency. The $B(M1)$ values are found to decrease with frequency which is reasonably well reproduced by TAC calculations. These $B(M1)$ values were also calculated using the Dönau-Frauendorf model [25], which assumes a fixed K value for the band and the alignments are perpendicular to the symmetry axis. The various parameters used in the calculations are listed in Table IV. The dot-dashed curve is obtained by assuming $(g_{7/2})^2$ configuration for neutrons. The calculated values for $(g_{7/2})(d_{5/2})$ configuration is about 33% higher. It is apparent from the plot that the measured $B(M1)$ values are better reproduced by the TAC calculation as compared to Dönau-Frauendorf estimate.

The measured $B(E2)$ transition rates in Band 1 have been listed in Table III. The corresponding $\mathcal{J}^{(2)}/B(E2)$ values for the three levels of Band 1 vary between 370 and 500 $\hbar^2\mathrm{MeV}^{-1}(e\mathrm{b})^{-2}$. The large $\mathcal{J}^{(2)}/B(E2)$ values also support that Band 1 in ^{104}Ag arises due to magnetic rotation. However, it is to be noted that large values of $\mathcal{J}^{(2)}/B(E2)$ are not unique indications of magnetic rotation [26].

B. Band 2

This nonyrast dipole band is a negative parity band with a bandhead at 12^- and could be established only up to $I^\pi = 16^-$. In addition, the present data are insufficient to extract any level lifetime in this band. Thus, it is difficult to ascertain the intrinsic configuration of Band 2.

From the arguments based on aligned angular momentum and parity, this band has been assigned $\pi[g_{9/2}] \otimes \nu[(g_{7/2}d_{5/2})^2\ h_{11/2}]$ configuration with neutron in unfavored $h_{11/2}$ orbital (*ABF* configuration). The values for deformation parameters β_2 and γ were found to be 0.09 and 31° for this configuration at $\hbar\omega = 0.3$ MeV.

The observed spins of Band 2 are plotted in Fig. 10 as a function of rotational frequency. The calculated $I(\omega)$ plot is shown by the dotted line. TAC calculations show a reasonable agreement with the slope of the experimental curve below $\hbar\omega = 0.45$ MeV. Beyond $\hbar\omega > 0.45$ MeV, the experimental data seem to indicate an onset of alignment. However, the band needs to be extended to higher spins in order to investigate this configuration beyond $\hbar\omega = 0.45$ MeV.

C. Band 3

The band 3 of ^{104}Ag has been assigned positive parity through PDCO measurements. In Fig. 11(a), the spins of the band are plotted as a function of rotational frequency. The figure shows the onset of an alignment around $\hbar\omega = 0.55$ MeV. A similar alignment has been observed in ^{109}Cd

TABLE IV. Parameters used in the calculation of $B(E1)$ transition rates.

Band	K	DAL configuration	$i_x^{(1)}(\hbar)$	$g^{(1)}$	RAL configuration	$i_x^{(2)}(\hbar)$	$g^{(2)}$
1[a]	4	$\pi[g_{9/2}]^{7+}_{2}$	1.5	+1.27	$\nu[h_{11/2}]^{1-}_{2}$	5.5	−0.21
1[b]	5	$\pi[g_{9/2}]^{7+}_{2}$	1.5	+1.27	$\nu([h_{11/2}]^{1-}_{2} \otimes [g_{7/2}]^{3+}_{2} \otimes [g_{7/2}]^{1+}_{2})$	11.5	0.063
3	5	$\pi[g_{9/2}]^{7+}_{2}$	1.5	+1.27	$\nu([h_{11/2}]^{1-}_{2} \otimes [h_{11/2}]^{3-}_{2} \otimes [g_{7/2}]^{1+}_{2})$	13.5	−0.063

[a]Configuration before alignment.
[b]Configuration after alignment.

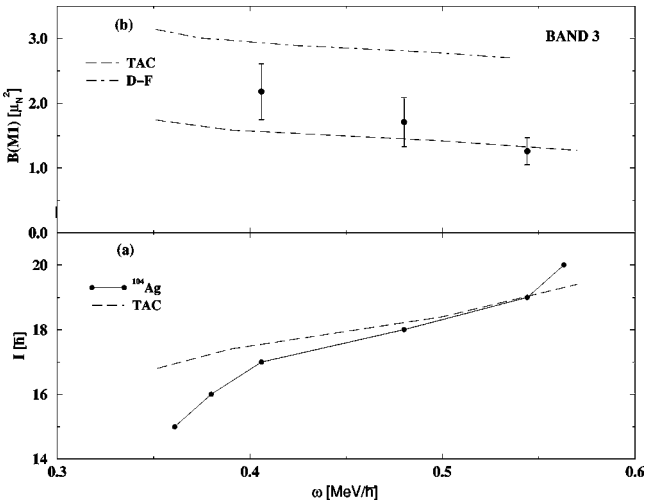

FIG. 11. (a) Angular momentum and (b) $B(M1)$ transition rates as a function of rotational frequency for Band 3. The explanation for various lines in the figure is same as in Fig. 9.

[2] and ^{108,110}In [9] and has been attributed to the *BC* crossing. Thus, the configuration after the crossing is $\pi[g_{9/2}] \otimes \nu[(g_{7/2}\ d_{5/2})^3\ (h_{11/2})^2$. However, as the present data fail to extend this band, no TAC calculation was performed to reproduce this crossing. The equilibrium values for β_2 and γ were found to be 0.18 and 25°, respectively, for $\pi[(g_{9/2})] \otimes \nu[(g_{7/2}\ d_{5/2})(h_{11/2})^2]$ configuration. The calculated $I(\omega)$ curves are shown by dashed curve in Fig. 11(a). There is a good agreement between the experimental and calculated values beyond $\hbar\omega = 0.4$ MeV while at lower frequencies the theory overestimates the observed spins.

The $B(M1)$ transition rates have been plotted as a function of rotational frequency in Fig. 11(b). The $B(M1)$ values decrease by a factor of 2 over the measured frequency range. The TAC calculation (shown in dashed curve) reproduces the $B(M1)$ values reasonably well. The Dönau-Frauendorf estimates for $\pi[(g_{9/2})] \otimes \nu[(g_{7/2})(h_{11/2})^2]$ configuration is shown in dash-dotted curve. The values calculated for $\pi[(g_{9/2})] \otimes \nu[(d_{5/2})(h_{11/2})^2]$ configuration is about 5% higher than the plotted values. It is evident from the figure that the TAC calculations give better agreement with the measured $B(M1)$ rates than Dönau-Frauendorf estimates. Thus, the good agreement between the observed features and the TAC calculations indicates the $M1$ character for this band.

VI. CONCLUSIONS

Two new nonyrast dipole bands (Bands 2 and 3) have been identified in odd-odd ^{104}Ag and their bandhead spins and parities were identified through DCO and PDCO measurements. The intrinsic configurations for the three observed bands were chosen such that they are consistent with observed parities and alignment characteristics of these bands. The deformation parameters for these configurations were extracted by minimizing the total Routhian. The $I(\omega)$ values from the TAC calculations for all the three bands show reasonable agreement with the experimental values. The lifetimes of the several levels of Bands 1 and 3 have been estimated from DSAM lifetime measurements. The $B(M1)$ rates in both Band 1 and 3 decrease with the increasing spin which is a signature of magnetic rotation and these rates are in better agreement with TAC calculations as compared to Dönau-Frauendorf estimates.

Thus, Bands 1 and 3 in ^{104}Ag exhibit all the features of a $M1$ band while Band 2 also seems to originate due to magnetic rotation but the present data are insufficient to confirm this assumption.

It is to be noted that both Bands 2 and 3 seem to indicate the onset of further alignments at the highest observable frequencies. Thus, these bands need to be extended further in order to investigate the nature of these alignments.

ACKNOWLEDGMENTS

The Clover array was set up at T.I.F.R. Pelletron jointly by T.I.F.R., Mumbai; S.I.N.P, Kolkata; IUC-DAEF, Kolkata; and N.S.C., New Delhi. The authors would like to thank all the participants in this joint national effort. Authors would also like to thank Dr. S. D. Paul for his participation during the data collection and all the technical staff of Pelletron for smooth operation of the machine.

[1] S. Frauendorf, Rev. Mod. Phys. **73**, 463 (2001); Nucl. Phys. **A557**, 259c (1993).
[2] C. J. Chiara *et al.*, Phys. Rev. C **61**, 034318 (2000).
[3] R. M. Clark *et al.*, Phys. Rev. Lett. **82**, 3220 (1999).
[4] A. Gadea *et al.*, Phys. Rev. C **55**, R1 (1998).
[5] D. G. Jenkins *et al.*, Phys. Lett. B **428**, 23 (1998).
[6] D. G. Jenkins *et al.*, Phys. Rev. C **58**, 2703 (1998).
[7] P. Vaska *et al.*, Phys. Rev. C **57**, 1634 (1998).
[8] P. Datta *et al.*, Phys. Rev. C **67**, 014325 (2003).
[9] C. J. Chiara *et al.*, Phys. Rev. C **64**, 054314 (2001).
[10] J. Treherne *et al.*, Phys. Rev. C **27**, 166 (1983).
[11] A. Goswami *et al.*, Z. Phys. A **353**, 231 (1995).
[12] M. Saha Sarkar *et al.*, Nucl. Instrum. Methods Phys. Res. A **491**, 113 (2002).
[13] D. C. Radford, Nucl. Instrum. Methods Phys. Res. A **361**, 297 (1995); Nucl. Instrum. Methods Phys. Res. A **361**, 306 (1995).
[14] K. Starosta *et al.*, Nucl. Instrum. Methods Phys. Res. A **423**, 16 (1999).
[15] J. C. Wells and N. R. Johnson (private communication).
[16] L. C. Northcliffe *et al.*, Nucl. Data, Sect. A **7**, 233 (1970).
[17] F. James *et al.*, Comput. Phys. Commun. **10**, 343 (1975).
[18] P. H. Regan *et al.*, Nucl. Phys. **A586**, 351 (1995).
[19] W. Nazarewicz *et al.*, Nucl. Phys. **A435**, 397 (1985).
[20] V. I. Dimitrov, S. Frauendorf, and F. Dönau, Phys. Rev. C **62**, 024315 (2000).

[21] Amita *et al.*, Phys. Rev. C **64**, 034304 (2001).
[22] A. H. Wapstra and G. Audi, Nucl. Phys. **A595**, 409 (1995).
[23] R. Bengtsson, S. Frauendorf, and F. R. May, At. Data Nucl. Data Tables **35**, 15 (1986).
[24] U. Dutta Pramanik *et al.*, Phys. Rev. C **52**, 117 (1995).
[25] F. Dönau, Nucl. Phys. **A471**, 469 (1987).
[26] R. M. Clark *et al.*, Annu. Rev. Nucl. Part. Sci. **50**, 1 (2000).